ARTICLES

Three-dimensional Ising system with long-range interactions: A computer model of Vycor glass

L. Monette, G. S. Grest, and M. P. Anderson
Corporate Research Science Laboratories, Exxon Research and Engineering Company, Annandale, New Jersey 08801
(Received 28 February 1994)

A computer model for Vycor glass using the three-dimensional Ising model with long range interactions is presented. The effect of the interaction range on the resulting Vycor microstructure is also investigated by measuring the pore size distribution for the $q=6$ (nearest neighbor) as well as longer-range interaction, i.e., $q=26$ and 124 Ising models. The discrepancy between the nearest-neighbor Ising model and the experimental results is interpreted in terms of a lattice-induced interfacial energy anisotropy. The influence of the range of interaction on the degree of interfacial energy anisotropy is illustrated by means of two- and three-dimensional Wulff plots (interfacial energy versus interface orientation) for each of the ranges of interaction considered. The shape of the pore size distributions obtained from the longer range Ising models is in agreement with the experimental results. However, the simulation distributions display a shift in the peak location observed as compared to the experimental distribution. The shift in peak location present in the simulation results is explained by a relative abundance of short chords combined with a lack of the large chords, with respect to the experimental results. This abundance of short chords is attributed to the interface roughness introduced by the longer range interaction, while the lack of large chords is attributed to the finite lattice sizes used in this study. A minimum system size and maximum interaction range are suggested, which should lead to a pore size distribution in close agreement with experimental results.

PACS number(s): 05.50.+q, 68.45.−v, 81.35.+k, 47.55.Mh

I. INTRODUCTION

Porous solids are critical to a variety of industrial applications, such as separation, oil recovery, heterogeneous catalysis, and even glass or ceramic processing [1]. Examples of such solids include polymer gels [2], polymer [3] and ceramics [4] membranes, cementitious materials and sedimentary rocks [2]. The common feature to all these materials is that they are complex interfacial media, i.e., they consist of two interpenetrating percolating phases: a solid and a porous phase having large surface to volume ratio. The presence of this large portion of interface between the pore and the solid phase introduces confinement, disorder, and often interactions such as wetting forces (adsorption), all of which may have a strong influence on the thermodynamics and/or the kinetics of processes taking place inside of such media [5]. In order to augment our understanding of the structure-property relationships for such materials, as well as eventually have the ability to synthesize by design porous materials with the desired selectivity, permeability, reactivity, or even catalytic properties, the first step and challenge is to characterize the morphology of such solids. The techniques used for this purpose are small angle (x-ray [6] or neutron [7] scattering (SAS), microscopy [6], molecular adsorption-desorption [8], and thermoporometry [9], to name a few. SAS probes the mass distribution correlations at various length scales, by measuring the structure factor. Direct mass distribution observation by way of an optical or electron microscope yields a chord size distribution. A chord is a linear path or segment comprised either inside the pore phase (pore chord) or inside the silica (solid chord) phase, connecting two distinct sites on the interface.

Vycor is a porous glass manufactured by Corning. The process for making this material begins with a high temperature single-phase melt of silica and boron oxide. The mixture is then quenched below its critical point, leading to the formation of silica rich and boron rich phases via spinodal decomposition. After some period of time, the obtained structure is quenched below the glass transition temperature, and the phase separation process ceases. The boron phase is subsequently leached out by acid, resulting in the final product, with a porosity of roughly 0.30. Vycor glass has recently been extensively studied [6–10] as a model material, for it possesses characteristics in common with porous materials of technological interest. Concurrently, the issue of how a porous medium alters the process of phase separation of a binary liquid mixture has also prompted a considerable amount of experimental [11–15] and theoretical [16–24] work. In these experiments, which focused on Vycor as a model porous medium, strong kinetics retardation as well as the absence of critical fluctuations in the vicinity of the critical point were observed. On the other hand, the theoretical and simulation work has provided useful but limited insight, since it has been carried out on idealized models. In particular, computer studies have been restricted to

two-dimensional interconnected tunnels [22], or a strip [24], or to a single pore in 3D [21], for lack of a reliable computer model of Vycor. The first objective of this work is to obtain a realistic computer model of Vycor, so theoretical understanding of the phase separation of liquid mixtures can be advanced by enabling the process to be simulated in a computer-generated 3D sample of porous medium with the same morphology as Vycor.

Since Vycor is produced by spinodal decomposition, it should be possible to obtain a computer model for Vycor using a coarse-grained model. However, realistic models for silica and boron oxide undergoing spinodal decomposition for all but the smallest samples, i.e., a few hundred atoms, is not feasible. The simplest model which shows spinodal decomposition is the Ising model. However, there exists two problems with this model. The first problem concerns the finite size of the lattice (i.e., how large a lattice is needed in order to obtain a statistically significant computer sample of Vycor). The second problem is related to the range of interaction, which if too short, causes high interface energy anisotropy [25]. This latter problem is of more serious concern, because a strong lattice-induced interfacial energy anisotropy results in a microstructure quite different than the one occurring in real systems, where the interfacial energy is isotropic. The approach followed in this work is to reduce the anisotropy of the 3D nearest-neighbor Ising model by extending the range of interaction, namely, from $q=6$ to 26 and 124 neighbors. The former problem is addressed by using as large a lattice as possible, in this case 128^3.

Crossley, Schwartz, and Banavar [26] developed a new class of three-dimensional (3D) geometrical models of porous media, based on the smoothing of random white noise images. However, these models suffer from the drawback of involving unknown smoothing parameters. One must therefore know beforehand the experimental results for the structure or transport properties in order to adjust these parameters. If the experimental information is already available, their approach is the easiest way to generate large computer samples of porous media, with linear sizes $L=256$ or more. In addition to the Ising model with conserved dynamics, other models which have been successfully used to investigate phase-ordering dynamics of first-order phase transitions include the coarse-grained Langevin model [27] and a cell dynamics version of model B [28]. Another interesting approach, the lattice-Boltzmann model [29], simulates the time evolution of immiscible fluids. Even though these models constitute valid approaches to obtain a computer model for "spinodally decomposed" solids such as Vycor, we have exclusively considered the 3D Ising model with longer range interactions so our findings can potentially be related to the considerable amount of Monte Carlo (MC) data on first-order phase transitions [30].

Binder and Stauffer [31] made the first theoretical prediction of the existence of a regime where the structure factor should exhibit scaling with respect to time. Most MC studies of scaling in first-order phase transitions have been carried out using the nearest-neighbor Ising model. Most of these studies [30,32] support scaling, as well as an asymptotic time dependence of the characteristic length, i.e., the inverse of the wave vector $\kappa^{-1}(t)$ at the peak of the structure factor, varying as $t^{1/3}$ for a conserved order parameter [33]. Some experimental results, however, show departures from this growth law [32]. Another study by Laradji and co-workers [34], investigating the dynamics of first-order phase transitions in 2D Ising models with a nonconserved order parameter but with long-range interactions, demonstrated the influence of the interaction range on the time of validity of the linear theory of spinodal decomposition. Their results support the predicted asymptotic scaling exponent of $\frac{1}{2}$ for a nonconserved order parameter independently of the interaction range chosen, as expected. The asymptotic behavior in the case of a conserved order parameter has been examined by Annett and Banavar [35] using an accelerated algorithm in which the global conservation of the order parameter is ensured by a Creutz demon [36]. This numerical simulation tehnique is a deterministic method due to Creutz. The demon and the lattice form a closed, isolated system with total magnetization M. Let M_d be the demon magnetization and M_s be the lattice magnetization. The demon generates a succession of configurations by distributing spins over the lattice, such that M_d and M_s can vary, with $M_d \ll M_s$, but $M=M_d+M_s$ must remain constant. A spin flip can be viewed as being equivalent to performing spin exchanges over very large ranges of interactions. They found an asymptotic growth exponent of $\frac{1}{2}$, which seems to suggest that systems with global conservation laws are in the same dynamic universality class as systems with no conservation laws. However, as the asymptotic growth exponent is indeed a property of the dynamical universality class, the range of interaction must affect nonuniversal amplitudes of the structure factor. Besides providing a computer model for Vycor, the second objective of this work is to develop a more physical picture for this idea by investigating the influence of the range of interaction on the microstructure itself, resulting from a spinodal decomposition process (conserved order parameter). This investigation is carried out in real space (as opposed to momentum space), as the microstructure is probed by way of the chord size distribution. As will be shown below, the physical picture brought in this work is based on the relation between the interaction range and the degree of anisotropy in the interfacial energy of the Ising model.

The organization of this paper is as follows: Sec. II describes the simulation model, as well as the procedure used to fabricate a sample of Vycor in the computer and to measure its chord size distribution. Section III describes how the interaction range in the Ising model is related to the degree of interfacial energy anisotropy, and presents the simulation results. Section IV summarizes our findings, and discusses our plans for future work.

II. SIMULATION MODEL

We briefly review the Ising model with long-range interactions. The demonstration of the unsuitability of the Ising model with nearest-neighbor interactions as a com-

puter model of Vycor is postponed to the next section. We make use of a three-dimensional simple cubic lattice with a spin σ_i at each vertex, where i labels the vertex, $\sigma_i = \pm 1$, and a_0 is the lattice spacing. The Hamiltonian for the 3D Ising model with $N = L^3$ sites is

$$\mathcal{H} = -\sum_{\langle ij \rangle} J_{ij}\sigma_i\sigma_j \ . \tag{2.1}$$

We use the equivalent neighbor model of Domb and Dalton [37] in Eq. (2.1), which was introduced as a way to bridge the gap between infinite range interaction (mean field theory) and short-range interactions. The interaction constant J_{ij} is modeled by a square well potential: J_{ij} is equal to $J > 0$ for all neighboring spins within a certain interaction range R and is zero for spins outside this range R. The lattice coordination number, $q = (2R+1)^3 - 1$ is therefore the number of lattice sites inside the square well. We consider two different ranges of interactions in this work, namely, $q = 26$ ($R = 1$) and $q = 124$ ($R = 2$). The product qJ is kept fixed, such that the limit $q \to \infty$, $J \to 0$ the model corresponds to the limit of mean field theory. Equation (2.1) becomes

$$\mathcal{H} = -\frac{1}{2}\sum_{i=1}^{N}\sum_{j \in nbh(i)}^{q} J\sigma_i\sigma_j \ , \tag{2.2}$$

where the summation of the first term is over all different $qN/2$ neighbor pairs $\langle ij \rangle$. Note that the Ising model with nearest-neighbor interactions has a lattice coordination number $q = 6$, and a critical point [38] at $k_B T_c / J \sim 4.50$, where k_B is the Boltzmann constant.

Periodic boundary conditions are imposed in all three directions. The systems considered in this work have linear size $L = 64$ and 128. The initial configuration is obtained by distributing at random the silica phase (70%) and the boron oxide phase (30%). The simulations using this initial configuration as a starting point are performed in the canonical ensemble, i.e., the concentration of each species is kept constant. We therefore make use of a more efficient variation of the Kawasaki algorithm, where pairs within the neighborhood defined by the interaction range are exchanged with the following probability:

$$p_i = \begin{cases} 1 & \text{if } \sigma_i = -\sigma_j \\ 0 & \text{otherwise} \end{cases} \tag{2.3a}$$

and acceptance rate

$$\mathcal{A}(\{\sigma\} \to \{\sigma'\}) = \min\left[1, \frac{\exp(-\beta\mathcal{H}\{\sigma'\})}{\exp(-\beta\mathcal{H}\{\sigma\})}\right] , \tag{2.3b}$$

where $\beta = 1/k_B T$, and σ' represents the spin configuration resulting from the exchange, with $\sigma_i' = \sigma_j$ and $\sigma_j' = \sigma_i$.

The system was quenched to $T = 0.45 T_c$, where T_c is the bulk critical point for the 3D Ising model with $q = 6$. This leads to the formation of a silica rich and boron-oxide-rich structure, by spinodal decomposition. If the simulation data are to be compared to the experimental results, then the spinodal decomposition process must be in the scaling regime, i.e., where the length scale of the problem (the average pore size) is much greater than the correlation length (which is no more than one or two lattice spacings a_0). The simulation is stopped at seven different times to obtain configurations in the scaling regime. We discuss below the criteria used to ensure that the selected configurations were in the scaling regime. Each configuration is further quenched another 1000 MCS (Monte Carlo Step per spin) at a very low temperature $T \sim 0.1 T_c$. The purpose of this second quench is to eliminate as much roughness as possible from the interface formed between the two phases. A cluster analysis which identifies all the clusters of both phases is then run for these frozen configurations. For the cluster analysis, the connectivity is limited to nearest neighbors only. Each configuration has one large percolating cluster made up of the boron oxide phase ($\sigma_i = 1$), which corresponds to the Vycor porous structure, one large percolating cluster made up of the silica phase ($\sigma_i = -1$), which corresponds to the silica background, and a few smaller clusters of each phase. In all the configurations analyzed, the largest boron-oxide cluster contains roughly 90% of all boron "atoms." This large boron-oxide cluster is an indication of the presence of an interconnected pore network. A large number of smaller clusters indicates that the pore network has pinched off into small domains which are individually coarsening. Also, the configurations are selected well before the interconnected pore structure becomes one single spherical cluster. For instance, the maximum average pore size considered for the $q = 124$, $L = 64$ system is $18a_0$, which is much less than the estimated average pore size of $50a_0$ in the case of a single spherical domain, assuming it contains roughly 30% of the sites. The process by which the boron-oxide phase is leached out from the real material is realized in the simulations in the following way. The smaller boron-oxide phase clusters, which are not connected to the largest one, are eliminated by flipping the spins so these clusters become part of the support. The cluster analysis is run again. There is now a single large boron-oxide cluster, a large silica cluster, and many smaller silica clusters. These smaller silica clusters which are embedded inside the boron-oxide cluster are removed along with the percolating boron-oxide phase, and treated as the "void" phase. The reason for this is that in the experimental process, the acid dissolves the boron-oxide phase, and presumably washes out small clusters of silica embedded in the boron structure. Therefore, the final porosity is not exactly 30%, but is close to its original value.

The pore chord size distribution of the final configurations is then measured. In the case of an infinite and isotropic material, measuring the chord size distribution along a given direction is sufficient to obtain a statistically significant sampling. These ideas do not quite apply here. As was discussed above, the square lattice is not isotropic, and the system linear sizes of 64 and 128 are far from what is considered infinite. The measurement of the chord distribution has to be modified in order to account for these nonideal conditions. Figure 1 illustrates the cubic lattice, where x-y (a), x-z (b), and y-z (c) planes are defined. The pore chord size distribution is measured for each of these planes (d) along lines drawn at angles taken in 40 different directions in the interval

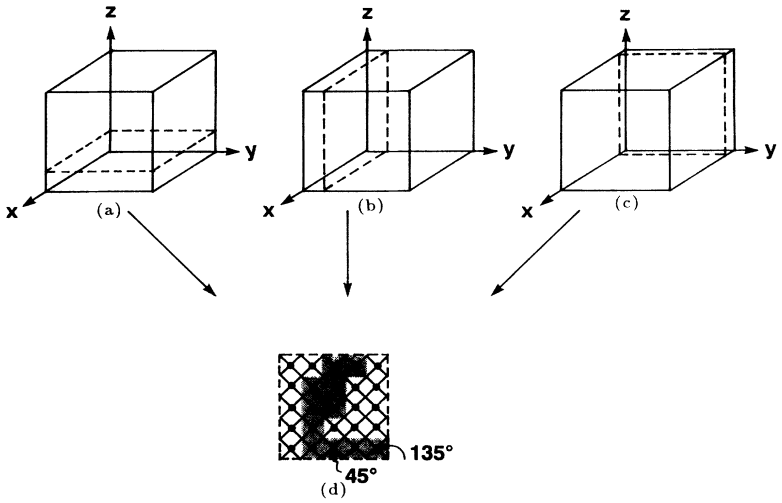

FIG. 1. Illustration of the cubic lattice with a cut along the (a) x-y, (b) x-z, and (c) y-z planes. The chord size distribution is measured for each of these planes (d) along lines drawn at angles taken in 40 different directions in the interval 0°–180°. (d) illustrates as an example a scan along the direction 45°-135° of a plane taken either from (a), (b), or (c). The squares represent the unit area per lattice point, and the gray squares represent the "empty" phase, while the white squares represent the silica phase. The chord lengths measured in this case by the lines at 45° are $2\sqrt{2}$, $3\sqrt{2}$, $2\sqrt{2}$, $\sqrt{2}$, $\sqrt{2}$, $\sqrt{2}$, and $\sqrt{2}$. The chord lengths measured by the lines at 135° are $\sqrt{2}$, $\sqrt{2}$, $\sqrt{2}$, $2\sqrt{2}$, $\sqrt{2}$, $\sqrt{2}$, $\sqrt{2}$, $2\sqrt{2}$, and $\sqrt{2}$.

0°–180°. Figure 1(d) illustrates as an example a scan along the direction $\theta=45°$ and 135° of a plane taken either from (a), (b), or (c). The squares represent the unit area per lattice point, and the gray squares represent the pore phase, while the white squares represent the silica phase. The frequency of occurrence of the pore chord lengths measured by this procedure is recorded, resulting in a pore size distribution. The average pore length l_{av} is obtained for each configuration. In the scaling regime, the length scale l_{av} must be greater than the correlation length $\xi=1-2a_0$. Consequently, the configurations are selected such that l_{av} is between 6 and $14a_0$ for $q=26$, and between 7 and $18a_0$ for $q=124$. As additional evidence for the scaling regime, we also verified that the chord size distribution obtained for each configuration, when rescaled by l_{av}, overlap one another. The pore size distribution shown in the next section for each interaction range considered represents an average over these seven configurations.

III. SIMULATION RESULTS

We first illustrate how the anisotropy of the interfacial energy for an Ising model on a square lattice is related to the range of interaction. The interfacial energy anisotropy is depicted in Fig. 2. Figures 2(a)–2(c) represent plots of the energy cost (γ) of a unit interface as a function of the interface orientation, normalized to the energy cost of an interface at 0°, in 2D. These plots have been obtained by numerically counting the number of nearest-neighbor "bonds" (in units of J) crossing a unit interface at an arbitrary angle, normalized to the number of bonds crossing a unit interface at 0°, leading to a dimensionless quantity γ. Figures 2(a) are for the first neighbor interactions only ($q=4$), 2(b) is for the first and second neighbor interactions ($q=8$), and 2(c) is for the first through fourth neighbor interactions ($q=20$). The coordinates are $\gamma\cos\phi$ and $\gamma\sin\phi$, where ϕ is the coordinate of the unit normal to the 2D interface (line). Figures 2(d)–2(f) are the same plot for a 3D lattice, with 2(d) for first neighbor ($q=6$), 2(e) for first through third neighbor ($q=26$), and 2(f) for first through eight neighbor ($q=124$) interactions, excluding the eight neighbors which fall outside of the range of interaction $R=2$. The full circles represent $\theta=10°$, the full squares, 20°, the full triangles 30°, the solid line 40°, the dotted line 50°, the dashed line 60°, the long-dashed line 70°, the dot-dashed line 80°, and the dot long-dashed line 90°, and the angles ϕ and θ represent the spherical polar coordinates of the unit normal to the 3D interface (plane). If the model were perfectly isotropic, this interface energy cost would be orientation invariant, i.e., one would obtain a circle (in 2D) or sphere (in 3D) of radius unity. Instead, one can note large cusps along certain directions in the interfacial energy plot for the Ising model with first neighbor interactions in both 2D and 3D. The surface cost along these directions is larger as a result of the anisotropy, therefore are suppressed by any energy-minimizing algorithm. The amplitude of these cusps decreases with increasing the range of interaction, i.e., from a maximal value of 41.42% for $q=4$ [Fig. 2(a)] to 5.29% for $q=8$ [Fig. 2(b)] to 3.48% for $q=20$ [Fig. 2(c)] for a 2D lattice; and from a maximal value of 74.53% (for a unit normal in the $\phi=45°$ and $\theta=55°$ direction) for $q=6$ [Fig. 2(d)] to 8.24% ($\phi=85$, $\theta=20$) for $q=26$ [Fig. 2(e)] and to 4.86% ($\phi=10$, $\theta=40$) for $q=124$ [Fig. 2(f)] for a 3D lattice. Note that the anisotropy in the nearest neighbor is considerably reduced by extending the range of interaction to the second (2D) or second and third neighbors (3D), but extending the range of interaction beyond that leads to very little improvement.

We now examine the microstructure resulting from the Ising model with longer range interactions, which we will qualitatively compare with that for the nearest-neighbor Ising model. Figure 3 shows a typical 2D cross section of the Vycor glass as obtained by the procedure detailed in Sec. II. Figures 3(a)–3(c) are for $q=26$, while 3(d)–3(f) are for $q=124$. The pore phase is white, while the silica background is black. Note how the main structure shown in Fig. 3(a) ($q=26$) grows preferentially in the directions 0° and 90°, i.e., along the x and y axes. This type of structure occurs frequently in Ising models with nearest-neighbor interactions. However, the degree of anisotropy in Figs. 3(a)–3(c) ($q=26$) is much less than for the nearest-neighbor interactions Ising model, i.e., 8.24% compared to 74.53%. This means that while this type of structure still occurs from time to time for $q=26$,

it is much less frequent than for the nearest-neighbor Ising model. Therefore, increasing the interaction range restores interfacial energy isotropy in the sense that a larger number of neighbors decreases the occurrence of preferential growth along x, y, and z axes.

Before proceeding with the simulation results, we present in Fig. 4 the experimentally-determined pore chord size distribution by Levitz and Tchoubar [6]. Their data were obtained by measuring the chord size distribution along random directions, using digitized images of Vycor cross sections. The authors estimated the accuracy of their chord size distribution measurement procedure to be good by checking it on basic figures, for which analytical expressions were available. However, the smaller chords whose size was less than the discrete unit (pixel) of the digital Vycor image could not be measured. Note the presence of a tail in the distribution at large chord sizes (greater than 200 Å). This tail implies

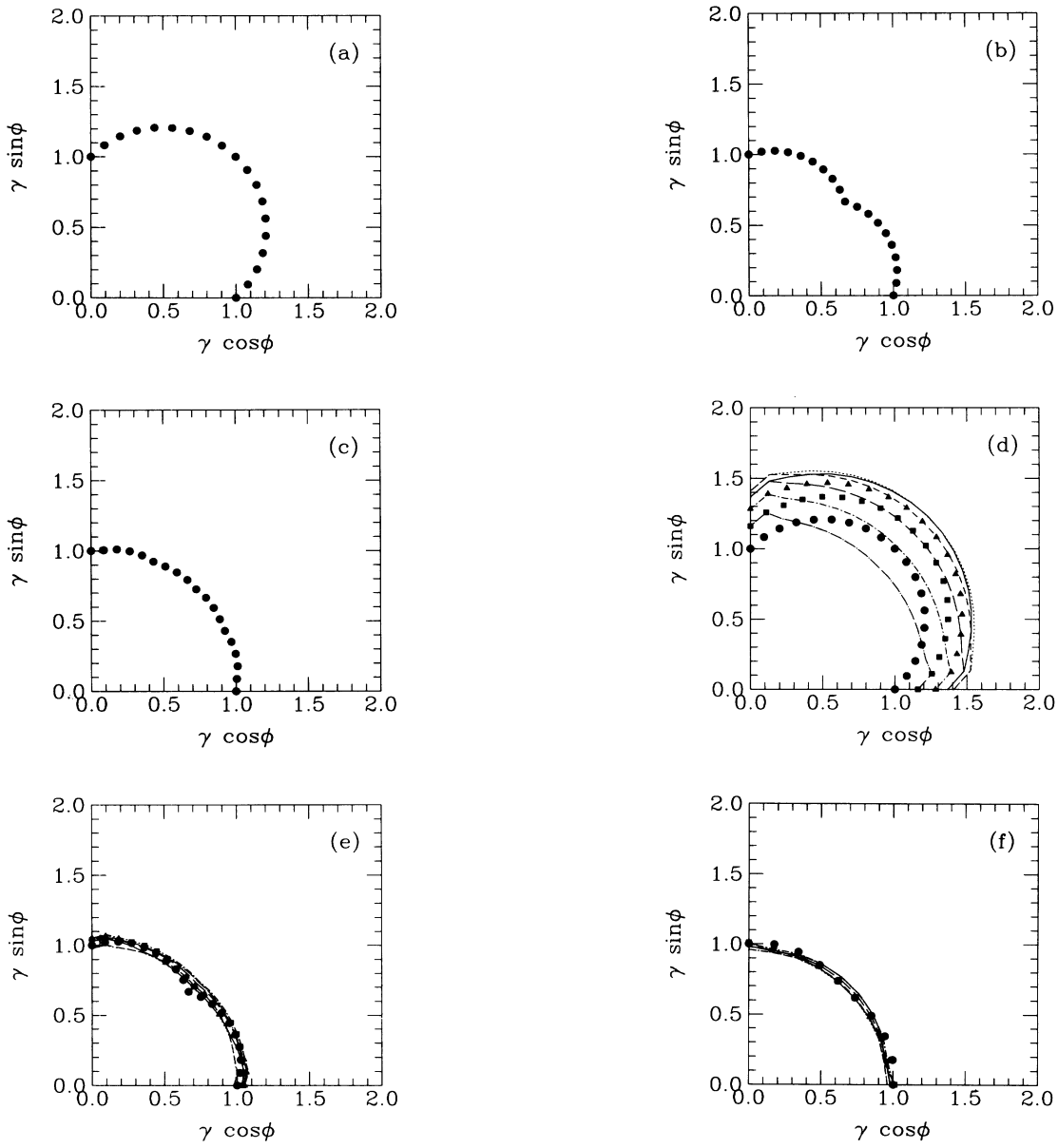

FIG. 2. (a)–(c) represent plots of the energy cost (γ) of a unit interface as a function of the interface orientation, normalized to the energy cost of an interface at 0°, in 2D. (a) is for first neighbor interactions only ($q=4$), (b) is for first and second neighbor interactions ($q=8$), and (c) is for first through fourth neighbor interactions ($q=20$). Here ϕ is the polar coordinate of the unit normal to the 2D interface (line). (d)–(f) are the same plot for a 3D lattice, with (d) for first neighbor ($q=6$), (e) for first through third neighbor ($q=26$), and (f) for first through eight neighbor ($q=124$) interactions, excluding the eight neighbors which fall outside of the range of interaction $R=2$. The full circles represent $\theta=10$, the full squares 20°, the full triangles 30°, the solid line 40°, the dotted line 50°, the dashed line 60°, the long-dashed line 70°, the dot-dashed line 80°, and the dot long-dashed line 90°, where the angles ϕ and θ represent the spherical polar coordinates of the unit normal to the 3D interface (plane).

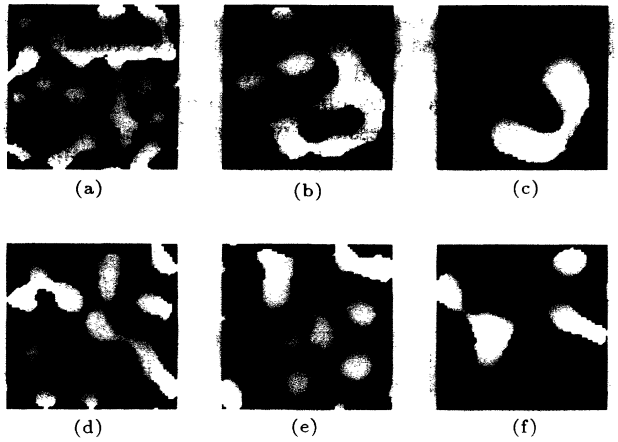

FIG. 3. 2D cross section of the Vycor glass as obtained from the Ising model with long-range interactions. (a)–(c) are for $q=26$, while (d)–(f) are for $q=124$. The pore phase is white, while the silica background is black.

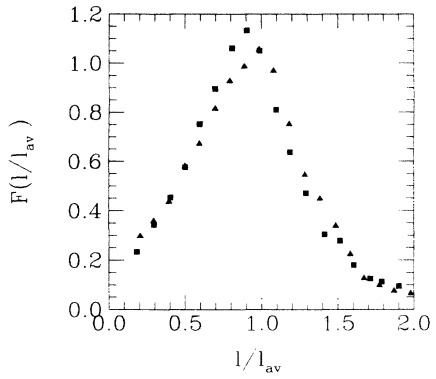

FIG. 5. The pore chord size distribution obtained from the long-range interaction Ising model and by measuring the lengths along directions parallel to the x-y-z axes (full triangles) versus the chord size distribution obtained by measuring along directions at 45°–135° (with respect to the axis), for a system with linear dimension $L=64$ and $q=124$. The chord length l (in units of lattice spacings) is scaled by l_{av}, where l_{av} is the average chord length, while the distribution is scaled to $f(l/l_{av})=l_{av}F(l)$. $f(l/l_{av})$ is normalized so that the area is unity.

that that average chord length (120 Å) is much greater than the chord length at the peak of the distribution (78 Å). The fact that chord sizes less than about 10 Å could not be measured, due to this resolution issue, might have also contributed to an average chord size value larger than would have otherwise been.

We now turn to the simulation data. First, we show in Fig. 5 the chord size distribution obtained by measuring the lengths along directions parallel to the x-y-z axes (full triangles) versus the chord size distribution obtained by measuring only along directions at 45°–135° with respect to the axis (full circles), for a system with linear dimension $L=64$ and $q=124$. $f(l/l_{av})$ is normalized so that the area is unity. The chord length is scaled by l_{av}, while the distribution is scaled to $f(l/l_{av})=l_{av}F(l)$. The data seem to lie for the most part on each other, except for the region close to the peak. Both the peak location and the peak height of the distributions showed roughly a 10% discrepancy from each other. This discrepancy seems to indicate a systematic trend, since each of these two chord distributions was averaged over seven configurations chosen at different times, in the scaling regime. Note that according to Fig. 2(f), the maximum anisotropy is 4.86% for an interaction range $q=124$. Consequently, the 10% discrepancy between the two directions in Fig. 5 cannot be due to lattice anisotropy only. We concluded that for $L=64$, the sample is not large enough, such that measuring the chord length in only one given direction or in a few random directions does not produce a statistically significant histogram. It was therefore decided to systematically measure the chord distribution in 40 different directions (as described in Sec. II), spanning the interval 0°–180°, in order to gather a histogram truly representative of the microstructure. In a similar way, the structure factor $S(q,t)$ is determined by all the wave vectors lying on a spherical shell of radius $|q|$, and not only by the wave vectors along the principal axis of the lattice. The rest of the chord size distribution data presented in this section has been obtained by this procedure.

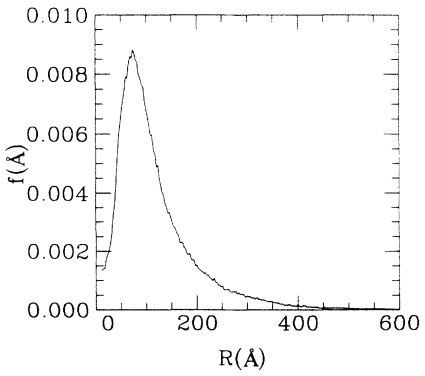

FIG. 4. The experimentally-determined pore chord size distribution by Levitz and Tchoubaur (see Ref. [6]). The chord size R unit in angstroms, while f is the frequency of occurrence of a chord of size R, normalized to the total number of chords.

Figure 6 displays the experimental pore chord size distribution, renormalized to $f(l/l_{av})$, keeping the area under the curve unity (solid line), the distribution obtained from a nearest-neighbor Ising model (dotted line), the distribution obtained from the $q=26$ (full triangles), and the $q=124$ (full circles) long-range Ising model with linear dimension $L=64$. The difference between the experimental results and the nearest-neighbor Ising results illustrates the effect of lattice-induced interfacial energy anisotropy on the resulting microstructure. Figure 2(d) suggests that a 3D lattice strongly constrains the growth to occur along the x-y-z axes. This suggests that the resulting pores possess a higher aspect ratio, i.e., the pore radius is much smaller than the distance between pore junctions, as this particular pore morphology would be consistent with the wide variation in chord sizes obtained by

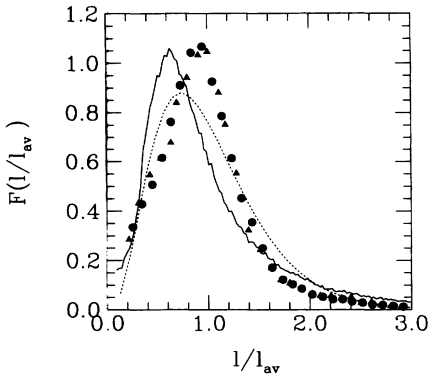

FIG. 6. Plot of the experimental chord size distribution [7], (solid line), the distribution obtained from a nearest-neighbor Ising model (dotted line), the distribution obtained from the $q=26$ (full triangles), and the $q=124$ (full circles) long-range Ising model with linear dimension $L=64$. The chord lengths for each distribution have been normalized to their respective average chord length, and all distributions have been normalized so their area is unity. The error (standard deviation) on each value $f(l/l_{av})$ is between 5 and 15%, and can be as large as 30% in the tail region ($l/l_{av} \geq 2$).

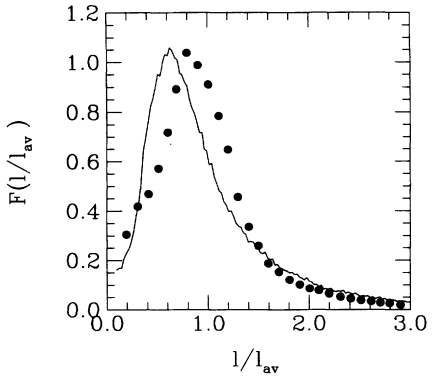

FIG. 7. Plot of the experimental chord size distribution [7] (solid line), as compared to the simulation chord size distribution (full circles) with $q=124$ and a system linear size $L=128$. The chord lengths for each distribution have been normalized to their respective average chord length, and all distributions have been normalized so their area is unity. The error (standard deviation) on each value $f(l/l_{av})$ is between 5 and 15%, and can be as large as 30% in the tail region ($l/l_{av} \geq 2$).

using the nearest-neighbor Ising model. As isotropy is restored to the interfacial energy by extending the range to include $q=26$ and 124 neighbors, the growth no longer occurs preferentially in the x-y-z directions, as the pores now grow in other directions at virtually the same energy cost. The isotropy of the interfacial energy may reduce the aspect ratio of the pores, such that the distance between pore junctions is now comparable to the pore diameter. This explanation can account for the narrower chord distribution obtained (see full triangles and squares). The fact that there is no difference detected in the pore size distribution obtained from a $q=26$ and a $q=124$ Ising model is in agreement with the surface energy plots in Figs. 2(e) and 2(f) where the maximum value calculated for the lattice anisotropy is 8.24% for $q=26$, versus 4.86% for $q=124$.

In spite of the fact that the shape of the chord size distribution curve obtained from the longer range Ising models compares very well with the experimental data, there is a notable shift in the peak location l_p, i.e., $l_p/l_{av}=0.625$ for the experimentally-determined chord size distribution versus 0.95 for the $q=26$ and 124 Ising models. This shift can be explained by the fact that the experimental data display fewer short chords but more large chords than the simulation data. The relative "lack" of short chords in the experimental data is at least partly due to difficulties in resolution. Chord lengths less than 10 Å are not observable, and this effect increases l_{av}, hence decreases l_p/l_{av}. On the other hand, the relative abundance of short chords in the simulation results could be due to an increased surface roughness introduced by a longer range of interaction. However, the lack of large chords in the simulation data is partially explained in terms of the small system size. Consequently, the presence of the large chords and the relative absence of the short chords in the experimental data bring the ratio $l_p/l_{av}=0.625$, while for the simulation data, the relative abundance of short chords and the lack of large chords increase that ratio close to unity, i.e., $l_p \sim l_{av}$.

In order to verify this last hypothesis, the pore chord size distribution is measured for a sample with linear size $L=128$. The result is displayed in Fig. 7. The solid line again represents the experimental chord size distribution, and the full circles represent the simulation chord size distribution with $q=124$. The abundance of small chords is still noticeable in the simulation results. In spite of that, the location of the peak has now shifted from 0.95 to slightly less than 0.80, indicating that the greater system size enables better large chord statistics.

IV. CONCLUSIONS AND FUTURE WORK

We obtained a computer model for Vycor by means of the 3D Ising model with long-range interactions. The chord size distribution was first measured along two distinct directions (0°-90° and 45°-135°) for a system with linear size $L=64$. A 10% discrepancy in both the peak height and location between the two distributions (each of them averaged over seven configurations) was found, in spite of the fact the lattice anisotropy in this case ($q=124$) is calculated to be 4.86%. This leads us to believe that part of this discrepancy is related to a sampling problem, and that measuring the chord lengths in 40 directions uniformly spanning the interval 0°–180° should improve the histogram statistics.

We compared the pore chord size distributions obtained by measurements along 40 directions in the interval 0°–180° (and averaged over seven configurations) for a system with linear size $L=64$ to the experimental and

nearest-neighbor Ising model results. It is found that the presence of longer-range interactions $q=26$ and 124 neighbors restores the interfacial energy isotropy, such that the shape of the obtained distributions is very close to the experimental one. The shape discrepancy between the nearest-neighbor Ising model chord size distribution and the experimental results was attributed to the strong lattice-induced interfacial energy anisotropy, calculated to reach a value as high as 74.53% along a plane with unit normal $\phi=45°$, $\theta=55°$ for the 3D Ising model with first neighbor interactions.

Two differences are found between the experimental and the long-range Ising model chord distributions. First, the model results seem to display a higher fraction of the short chords than the experimental results. Keeping in mind that a resolution problem in the digitization of the Vycor cross-section pictures could have contributed to this discrepancy, a possible explanation is that the longer-range interactions introduce surface roughness. If it is the case, interaction ranges greater than $q=124$ should definitively not be used, so the interfaces between the pore and silica phases remain sharp enough. Second, the model results display a lack of large chords, as compared to the experimental results. This last discrepancy is related to the finite size of the simulation system, which prevents a statistically significant sampling of the very large pore sizes. These two differences contributed to a shift in the location of the peak, l_p/l_{av}, which was around 0.625 for the experimental distribution versus 0.95 for the long-range Ising model results with $L=64$. Increasing the system size to $L=128$ improved the larger pore statistics, such that the peak position l_p/l_{av} dropped to a value of about 0.8. This last distribution also showed a larger proportion of short chords as compared to the experimental one. Since this distribution was obtained with the $q=124$ interaction range, we propose that surface roughness induced by the longer interaction range is the cause of this large proportion of small chords. We conclude that lattices with a linear dimension of at least 256 and higher, with an interaction range not exceeding first, second, and third neighbors ($q=26$) are expected to yield chord size distributions in agreement with experimental results. Future work includes, in particular, the investigation by means of simulations of the kinetics behavior of phase separation of a binary liquid mixture trapped in the computer model for Vycor developed in this study.

ACKNOWLEDGMENTS

We would like to express our gratitude to W. Klein for his suggestions, from which this work benefited greatly. We are also grateful to S. K. Sinha and M. Y. Lin for useful discussions and comments.

[1] F. A. Dullien, *Porous Media: Fluid Transport and Pore Structure* (Academic, New York, 1976).

[2] *Physical Phenomena in Granular Materials,* edited by G. D. Cody, T. H. Geballe, and P. Sheng, MRS Symposium Proceedings No. 195 (Materials Research Society, Pittsburgh, PA, 1990).

[3] *Inorganic Membranes Synthesis, Characteristics and Applications* (Reinhold, New York, 1991).

[4] *Membrane Handbook,* edited by W. S. Ho and K. K. Sirkar (Reinhold, New York, 1992).

[5] J. Klafter and J. M. Drake, *Molecular Dynamics in Restricted Geometries* (Wiley, New York, 1989).

[6] P. Levitz and D. Tchoubar, J. Phys. I (France) **2**, 771 (1992).

[7] M. Y. Lin and S. K. Sinha, *Physical Phenomena in Granular Materials* (Ref. [2]), p. 485.

[8] R. S. Mikhail, S. Brunauer, and E. E. Bodor, J. Colloid Interface Sci. **26**, 45 (1968).

[9] M. Brun, A. Lallemand, J.-F. Quinson and C. Eyraud, Thermochim. Acta **21**, 59 (1977); J.-F. Quinson and M. Brun, in *Characterization of Porous Solids,* edited by K. K. Unger, J. Rouquerol, K. S. W. Sing, and K. Kral (Elsevier, Amsterdam, 1988), p. 307.

[10] P. Levitz and J. M. Drake, Phys. Rev. Lett. **58**, 686 (1987); P. Levitz, G. Ehret, S. K. Sinha, and J. M. Drake, J. Chem. Phys. **95**, 6151 (1991); B. Abeles, L. F. Chen, J. W. Johnson, and M. F. Drake, *Physical Phenomena in Granular Materials* (Ref. [2]), p. 491.

[11] M. C. Goh, W. I. Goldburg, and C. M. Knobler, Phys. Rev. Lett. **58**, 1008 (1987).

[12] W. I. Goldburg, in *Physics of Complex and Supermolecular Fluids,* edited by S. A. Safran and N. A. Clark (Wiley, New York, 1987), p. 475.

[13] S. B. Dierker and P. Wiltzius, Phys. Rev. Lett. **58**, 1865 (1987); P. Wiltzius, S. B. Dierker, and B. S. Dennis, *ibid.* **62**, 804 (1989); S. B. Dierker, B. S. Dennis, and P. Wiltzius, *ibid.* **66**, 1185 (1991).

[14] M. Y. Lin, S. K. Sinha, J. M. Drake, X. L. Xu, and P. Thiyagarajan, Phys. Rev. Lett. (1994).

[15] Y. P. Handa, M. Zakrzewski, and C. Fairbridge, J. Phys. Chem. **96**, 8594 (1992).

[16] F. Brochard and P. G. de Gennes, J. Phys. Lett. (Paris) **44**, 785 (1983); P. G. de Gennes, J. Phys. Chem. **88**, 6469 (1984).

[17] D. Andelman and J. F. Joanny, *Scaling Phenomena in Disordered Systems,* edited by R. Pynn and A. Skjeltorp (Plenum, New York, 1985).

[18] D. A. Huse, Phys. Rev. B **36**, 5383 (1987).

[19] A. Maritan, M. R. Swift, M. Cieplak, M. H. W. Chan, M. W. Cole, and J. R. Banavar, Phys. Rev. Lett. **67**, 1821 (1991).

[20] A. J. Liu, D. J. Durian, E. Herbolzheimer, and S. A. Safran, Phys. Rev. Lett. **65**, 1897 (1990).

[21] A. J. Liu and G. S. Grest, Phys. Rev. A **44**, R7894 (1991); L. Monette, A. J. Liu, and G. S. Grest, *ibid.* **46**, 7664 (1992).

[22] J. C. Lee, Phys. Rev. B **46**, 8648 (1992); Phys. Rev. Lett. **70**, 3599 (1993).

[23] A. Chakrabarti, Phys. Rev. Lett. **69**, 1548 (1992).

[24] A. Bhattacharya, M. Rao, and A. Chakrabarty, Phys. Rev.

E **49**, 524 (1994).
[25] D. J. Srolovitz, M. P. Anderson, G. S. Grest, and P. S. Sahni, Scr. Metall. **17**, 241 (1983).
[26] P. A. Crossley, L. M. Schwartz, and J. R. Banavar, Appl. Phys. Lett. **59**, 3553 (1991).
[27] K. R. Elder, T. M. Rogers, and R. C. Desai, Phys. Rev. B **38**, 4725 (1988).
[28] Y. Oono and S. Puri, Phys. Rev. Lett. **58**, 836 (1987); Phys. Rev. A **38**, 434 (1988).
[29] A. K. Gunstensen, D. H. Rothman, S. Zaleski, and G. Zanetti, Phys. Rev. A **43**, 4320 (1991).
[30] J. D. Gunton, M. San Miguel, and P. S. Sahni, in *Phase Transitions and Critical Phenomena,* edited by C. Domb and J. L. Lebowitz (Academic, London, 1983), Vol. 8, p. 374, and references therein.
[31] K. Binder and D. Stauffer, Phys. Rev. Lett. **33**, 1006 (1974).
[32] K. Binder, *Material Science and Technology: Phase Transformation in Materials,* edited by R. W. Cahn, P. Haasen, and E. J. Kramer (VCH, Weinheim, 1991), Vol. 5, Chap. 7.
[33] D. Huse, Phys. Rev. B **34**, 7845 (1986); J. G. Amar, F. E. Sullivan, and R. D. Mountain, *ibid.* **37**, 196 (1988); A. Chakrabarti, R. Toral, and J. D. Gunton, Phys. Rev. E **47**, 3025 (1993).
[34] M. Laradji, M. Grant, M. J. Zuckermann, and W. Klein, Phys. Rev. B **41**, 4646 (1990).
[35] J. F. Annett and J. R. Banavar, Phys. Rev. Lett. **68**, 2941 (1992).
[36] M. Creutz, Phys. Rev. Lett. **50**, 1411 (1983).
[37] C. Domb and N. W. Dalton, Proc. Phys. Soc. London **89**, 859 (1966).
[38] A. J. Wakefield, Proc. Cambridge Philos. Soc. **47**, 419 (1951).

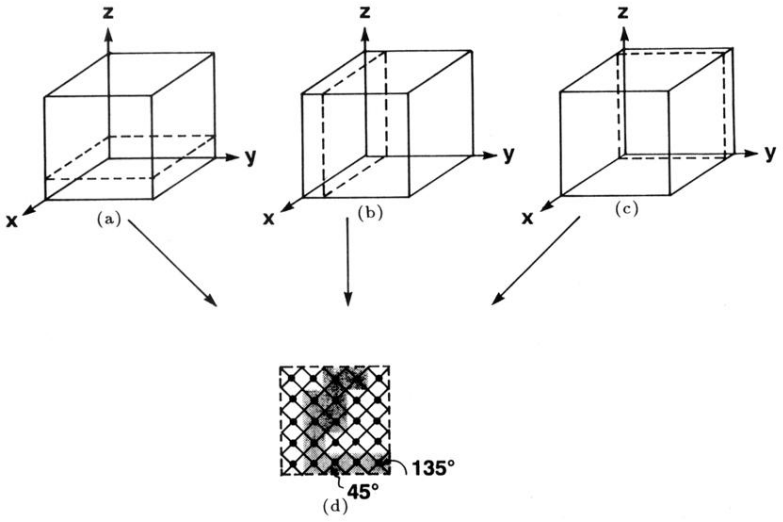

FIG. 1. Illustration of the cubic lattice with a cut along the (a) x-y, (b) x-z, and (c) y-z planes. The chord size distribution is measured for each of these planes (d) along lines drawn at angles taken in 40 different directions in the interval 0°–180°. (d) illustrates as an example a scan along the direction 45°-135° of a plane taken either from (a), (b), or (c). The squares represent the unit area per lattice point, and the gray squares represent the "empty" phase, while the white squares represent the silica phase. The chord lengths measured in this case by the lines at 45° are $2\sqrt{2}$, $3\sqrt{2}$, $2\sqrt{2}$, $\sqrt{2}$, $\sqrt{2}$, $\sqrt{2}$, and $\sqrt{2}$. The chord lengths measured by the lines at 135° are $\sqrt{2}$, $\sqrt{2}$, $\sqrt{2}$, $2\sqrt{2}$, $\sqrt{2}$, $\sqrt{2}$, $\sqrt{2}$, $2\sqrt{2}$, and $\sqrt{2}$.

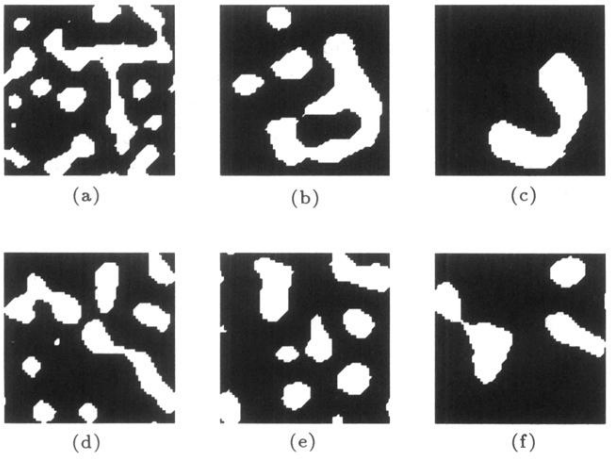

FIG. 3. 2D cross section of the Vycor glass as obtained from the Ising model with long-range interactions. (a)–(c) are for $q=26$, while (d)–(f) are for $q=124$. The pore phase is white, while the silica background is black.